Int. J. Electrochem. Sci., 15 **(2020)** 9669 – 9682, doi: 10.20964/2020.10.31

International Journal of ELECTROCHEMICAL SCIENCE
www.electrochemsci.org

A Novel Electrochemical Impedance Immunosensor for Aflatoxin B1 Based on L-cysteine Self-Assembled on Au Nanoparticles-Porous Nitrogen Doped Graphene Modified Electrode

Aiping Fan[1], *Ling Shi*[1], *Hongping Yang*[2] *and Guangming Yang*[1,*]

[1] Engineering Research Center for Processing and Quality Control of Local Characteristic Food and Consumer Goods of High Education in Yunnan Province, College of Science, Honghe University, Mengzi 661199, PR China
[2] Library, College of Science, Honghe University, Mengzi 661199, PR China
[*]E-mail: yangguangmingbs@126.com

Received: 3 June 2020 / *Accepted:* 28 July 2020 / *Published:* 31 August 2020

This work reports a novel electrochemical impedance immunosensor for aflatoxin B1 (AFB1) based on L-cysteine, Au nanoparticles (Au NPs), and porous nitrogen-doped graphene (P-N-r-GO). P-N-r-GO was prepared via the hydrothermal method using 4-aminopyrazolo[3,4-d]pyrimidine as a novel nitrogen source, which was then oxidized in the presence of HNO_3 to form a porous structure. Au NPs were electrodeposited on P-N-r-GO modified glassy carbon electrode (GCE). Then, L-cysteine was self-assembled onto the surface of Au NPs with its thiol group, and its amino group and carboxyl group were simultaneously used to covalently combine AFB1 antibody as the same group on the modified electrode using the bidirectional covalence strategy. Finally, an electrochemical immunosensor was constructed using $Fe(CN)_6^{3-/4-}$ to produce impedance signal. The sensor proved to be an excellent sensing platform for AFB1 by exhibiting a linear range of 0.01 ng mL^{-1} to 10 ng mL^{-1} with a detection limit of 0.001 ng mL^{-1}.

Keywords: Electrochemical sensor; Porous N doped graphene; L-cysteine; Au nanoparticles; 4-Aminopyrazolo[3,4-d]pyrimidine

1. INTRODUCTION

Aflatoxins (AFTs) are highly toxic mycotoxins produced by fungi that widely exist in mildewed foodstuffs and are detrimental to human health as they are highly carcinogenic, mutagenic and teratogenic even at very low concentrations [1]. Among these, alfatoxin B1 (AFB1) is the most toxic type, and in most countries, food safety programs strictly establish its maximum tolerable level at

2 ~ 20 μg kg^{-1} [1]. Consequently, constructing a simple, selective and sensitive method to measure AFB1 level is of significant importance.

Currently, various analytical methods, including ultra-high performance liquid chromatography-mass spectrometry (ultra-HPLC-MS) [2-4], enzyme-linked immunosorbent assay (ELISA) [5, 6] and electrochemical sensor [7-9], are used to detect AFB1 levels in food samples. Among these methods, electrochemical sensors are promising due to their attractive properties such as low-cost, fast operation and highly sensitivity [1]. The crucial step in developing electrochemical sensors is the immobilization of the recognition receptor, such as an antibody or an aptamer, on the electrode surface to form a sensing interface. To enhance selectivity, conductive nanomaterials with large surface area, such as carbon materials and their functionalized derivatives [10-13], conductive polymers [7, 10, 14] and metal nanoparticles (NPs) [1, 12, 15], are commonly used as carriers to immobilize the recognition receptor. Self-assembly and covalent bonding are the two main strategies to achieve this process. For the former, thiol or amino group of the recognition receptor self-assembles on noble metal NPs [12, 15, 16]. For the latter, amino group or carboxyl group of the recognition receptor covalently bonds to the carrier as same groups [10, 13]. In this regard, the porous and three-dimensional structure is advantageous as it possesses excellent mass transfer and electron transfer in comparison to others, such as Ag NPs hybridized mesoporous carbon [15], carbon nanotubes hybridized chitosan [17], carbon nanotubes-poly(diallyldimethylammoniumchloride)-Pd-Au NPs [12] and poly(3,4-ethylenedioxythiophene)-Au NPs [18]. Thus, it is essential to design a new immobilization strategy for the recognition receptor with a porous and three-dimensional carrier.

Nitrogen-doped graphene (N-r-GO) is a promising material for electrochemical sensors as N-doping effectively improves catalytic activity, enhances pore affinity to aqueous electrolytes, and reduce electric resistance compared to r-GO [19, 20]. N-r-GO can be synthesized employing various methods including chemical vapor deposition, thermal annealing, acid catalysis and hydrothermal method [19]. The hydrothermal method is a popular strategy to prepare the large-scale N-r-GO, and thus various nitrogen-containing organic compounds have been used widely in this field [21-24], but it is still important to broaden its nitrogen source.

This work uses 4-aminopyrazolo[3,4-d]pyrimidine as a novel nitrogen source to prepare N-r-GO via the hydrothermal method, and uses HNO_3 to oxidize it to obtain porous N-r-GO (P-N-r-GO). Then, Au NPs are electrodeposited on P-N-r-GO modified glassy carbon electrode (GCE). Then, L-cysteine is self-assembled on Au NPs surface with its thiol group. The amino and carboxyl groups of L-cysteine are simultaneously used to covalently link AFB1 antibody to the modified electrode. To the best of our knowledge, this work uses 4-aminopyrazolo[3,4-d]pyrimidine for the first time as a nitrogen source to prepare N doped r-GO in the hydrothermal method. Furthermore, this is also the first time the amino and carboxyl groups of AFB1 antibody are adopted to covalently bind L-cysteine as the same groups on Au NPs surface, which can improve the amount of AFB1 antibody in comparison to unidirectional strategy.

2. EXPERIMENTAL

2.1. Apparatus and reagents

Apparatus and reagents are given in Supplementary Information (**SI**). Graphene oxide (GO) was prepared using the modified Hummers method [25] and characterized as in our previous work [26].

2.2. Preparation of N-r-GO and P-N-r-GO

N-r-GO was prepared via the hydrothermal method using 4-aminopyrazolo[3,4-d]pyrimidine as a novel nitrogen source. 0.1 g GO was ultrasonicated for 60 min to prepare a 1 mg mL^{-1} aqueous GO suspension. Then, 30 mg 4-aminopyrazolo[3,4-d]pyrimidine was dissolved in the GO suspension, and the obtained mixture was transferred into a 150 mL Teflon-lined stainless steel autoclave to carry out the hydrothermal reaction at 250 °C for 12 h. The obtained product was centrifuged, and washed with purified water and ethanol, respectively, followed by freeze-drying for 24 h. As a result, N-r-GO was obtained. Finally, as explained in SI, it was oxidized using HNO_3 to form P-N-r-GO.

2.3. Construction of the sensor and its electrochemical characterization

Scheme 1 illustrates the proposed process for the construction of the sensor. Firstly, 5 µL of 1 mg L^{-1} P-N-r-GO was put on a clean GCE surface, and dried under an infrared lamp. Then, it was immersed in a 10 mL electrolyte consisting of 10 mmol L^{-1} $HAuCl_4$ and 0.1 mol L^{-1} $HClO_4$, and electrodeposited at -0.5 V for 20 s to obtain Au NPs / P-N-r-GO / GCE. The obtained electrode was washed with purified water, and immersed in a 0.1 mol L^{-1} L-cysteine for self-assembly. After 1 h, L-cysteine-Au NPs / P-N-r-GO / GCE was activated with a 0.4 mol L^{-1} N-(3-dimethylaminopropyl)-N'-ethylcarbodiimide (EDC) and 0.1 mol L^{-1} N-Hydroxysulfosuccinimide (Sulfo-NHS) in PBS (pH=7.2) for 20 min at room temperature. At the same time, a 150 µg mL^{-1} AFB1 antibody was activated at the same conditions. The electrode was washed with PBS (pH= 7.2), and immersed in a 40 µL of 150 µg mL^{-1} AFB1 antibody to carry out covalent reaction for 4 h to obtain AFB1 anti-L-cysteine-Au NPs / P-N-r-GO / GCE. Then, it was immersed in a 40 µL of 2.5 % BSA for 40 min in order to block the nonspecific sites. Finally, an electrochemical immunosensor was fabricated using $Fe(CN)_6^{3-/4-}$ to produce the impedance signal. For comparison, only AFB1 antibody was activated at the same conditions to construct an immunosensor, and AFB1 antibody was directly self-assembled on Au NPs surface with its amino-group to prepare another immunosensor at the same conditions except in the absence of L-cysteine.

Next, the obtained AFB1 anti-L-cysteine-Au NPs / P-N-r-GO / GCE was immersed in a AFB1 solution to detect AFB1 for 70 min at 37 °C, and then it was washed with PBS (pH= 7.2) and purified water, respectively. The obtained electrode was then used as the working electrode in a three-electrode measurement in an electrolyte consisting of 1.0 mmol L^{-1} $K_3Fe(CN)_6$+$K_4Fe(CN)_6$ and 0.1 mol L^{-1} KCl.

Finally, electrochemical impedance spectroscopy (EIS) measurement was conducted in the frequency range of 0.1 Hz to 100 kHz, and the electron-transfer resistance (Ret) was used as the response value.

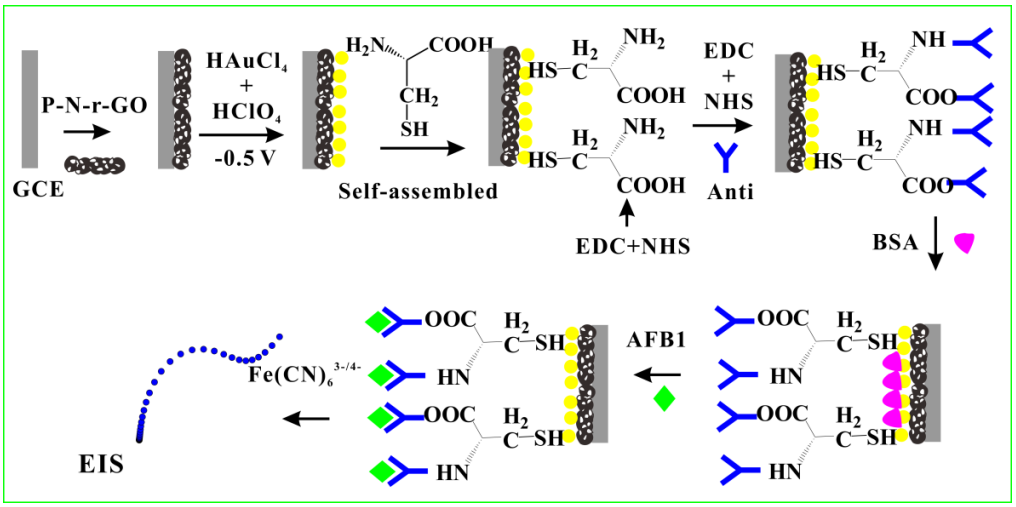

Scheme 1. The Scheme for preparation of immunosensor

3. RESULTS AND DISCUSSION

3.1 Characterization for N-r-GO and P-N-r-GO

The TEM image in Fig. 1A depicts the characteristic wrinkled structure of N-r-GO, and EDS mapping demonstrates successful nitrogen doping in r-GO (Fig. S1). N-r-GO exhibits a porous structure after oxidation with HNO_3 with an average pore size of 10 nm (Fig. 1B), and its EDS mapping image records distribution of C, N and O (Fig. 1C-F). X-ray photoemission spectroscopy (XPS) survey spectra further confirm the bond configurations of the nitrogen atoms (Fig. 1G) where C 1s peak, N 1s peak and O 1s peak were found at 284.59 eV, 399.79 eV and 531.94, respectively, which was consistent with the results obtained in the literature using the similar method [21], and the percentages of C, O, and N in P-N-r-GO were calculated as 85.60%, 11.06% and 3.34%, respectively.

The sp2 carbon atoms (C1) was found at 284.50 eV, and the other two weak peaks were centered at 285.50 eV, 288.50 eV (Fig. S2A), corresponding to the sp3 C, C-N and C-O, respectively. Meanwhile, three different N types with binding energies of 398.40, 399.90, and 401.30 eV were identified, corresponding to the pyridinic N, pyrrolic N, and graphitic N, respectively (Fig. S2B).

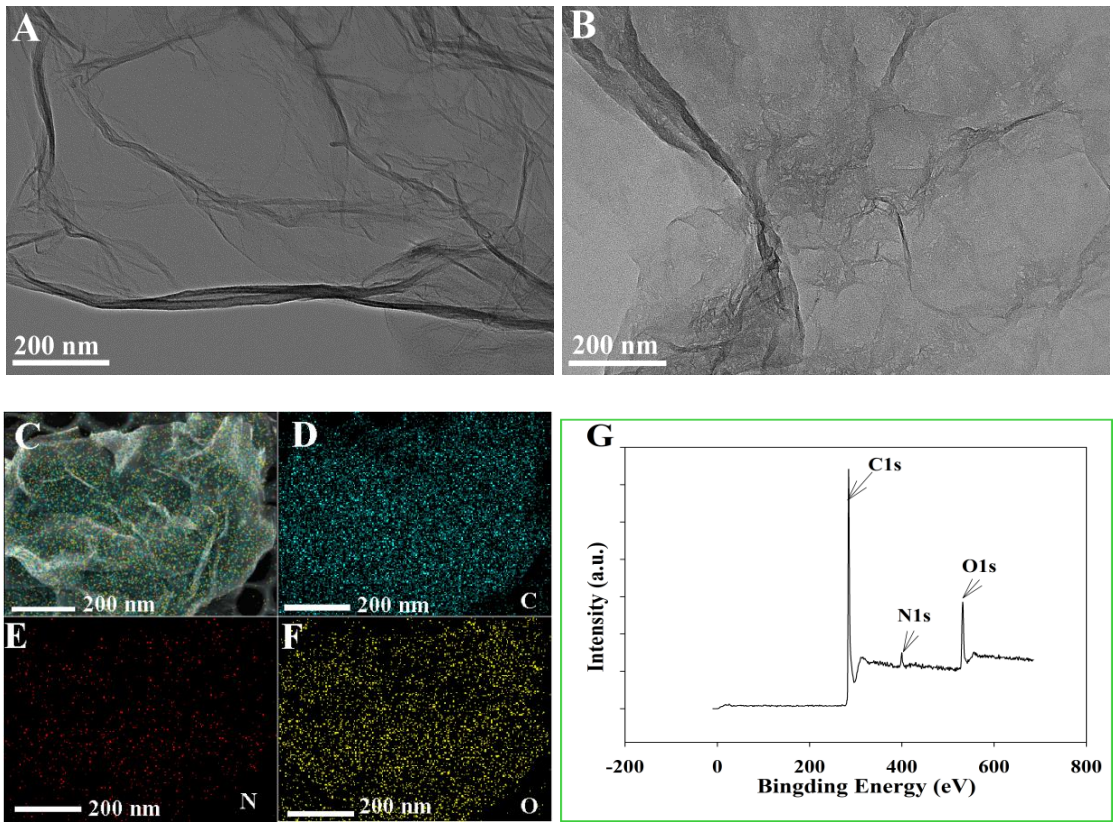

Figure 1. TEM images of N-r-GO (A) and P-N-r-GO (B), and EDS mapping of P-N-r-GO (C-F), and XPS survey spectra of P-N-r-GO (G).

3.2 Characterization of electrochemical immunosensor

SEM image of P-N-r-GO / GCE were depicted in Fig. 2A illustrating the three-dimensional structure. After an electrodeposition of 20 s, massive Au NPs with diameters between 50 ~ 80 nm were electrodeposited on the P-N-r-GO surface (Fig. 2B), meaning this interface could provide more surface areas to assemble L-cysteine.

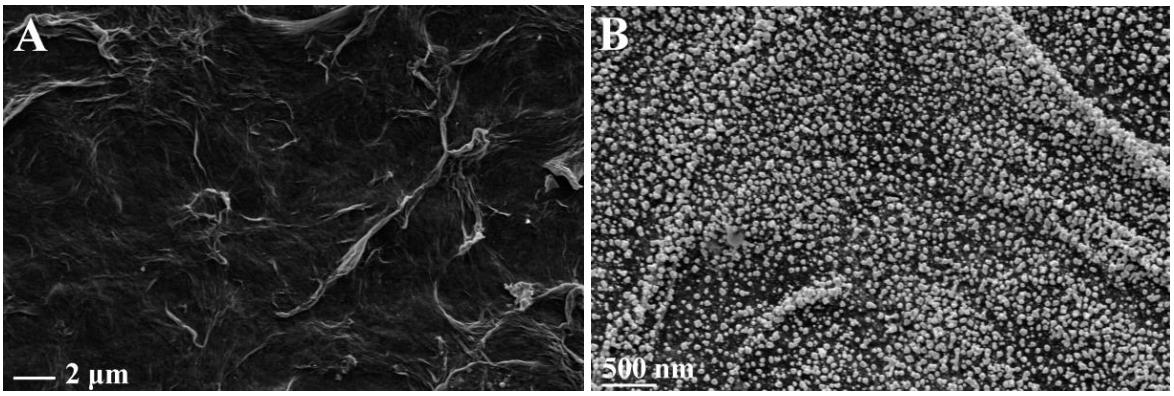

Figure 2. SEM images of P-N-r-GO / GCE (A) and Au NPs- P-N-r-GO / GCE(B).

Next, EIS was used to characterize the change of the interfaces for the fabrication of the immunosensor (Fig. 3). The Ret of GCE was measured as approximately 1500 Ω (Fig. 3A(a)). When P-N-r-GO was modified on CGE (Fig. 3A(b)) and Au NPs were electrodeposited on P-N-r-GO surface (Fig. 3A(c)), the EISs presented almost a straight line (Fig. 3A(b-c)) which was attributable to the excellent conductivity of P-N-r-GO and Au NP. When L-cysteine was self-assembled on the Au NPs surface, the Ret increased to 800 Ω (Fig. 3B(a)), indicating that L-cysteine enhanced the impedance of the modified electrode, which was similar to the results as the same strategy [27]. Meanwhile, when AFB1 antibody was covalently bonded to L-cysteine, the Ret of AFB1 anti-L-cysteine-Au NPs-P-N-r-GO / GCE reached 2450 Ω (Fig. 3B(b)) indicating the immobilization of the AFB1 antibody on the electrode. When BSA was used to block the nonspecific sites, the Ret of the electrode was 3500 Ω (Fig. 3B(c)). As a result, an electrochemical immunosensor for AFB1 was successfully constructed. Finally, when the sensor was tested in 0.50 ng mL^{-1} AFB1, the Ret was measured as 7020 Ω (Fig. 3B(d)) indicating the proper functioning of the immunosensor.

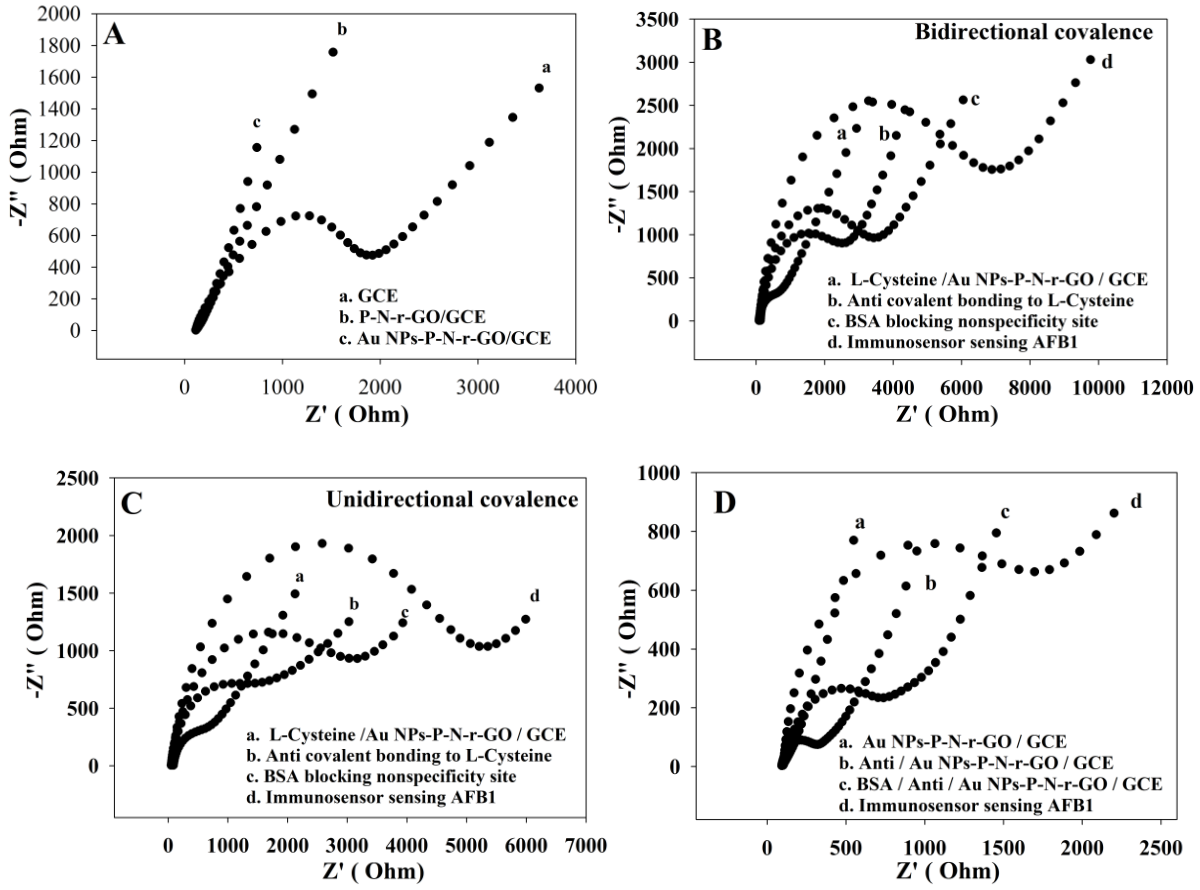

Figure 3. (A) EIS of GCE (a), P-N-r-GO / GCE (b) and Au NPs-P-N-r-GO / GCE in 1.0 mmol L^{-1} $K_3Fe(CN)_6$+$K_4Fe(CN)_6$ containing 0.1 mol L^{-1} KCl. (B) EISs of immunosensor prepared with bidirectional covalence in 1.0 mmol L^{-1} $K_3Fe(CN)_6$+$K_4Fe(CN)_6$ containing 0.1 mol L^{-1} KCl. (C) EISs of immunosensor prepared with unidirectional covalence in 1.0 mmol L^{-1} $K_3Fe(CN)_6$+$K_4Fe(CN)_6$ containing 0.1 mol L^{-1} KCl. (D) EISs of immunosensor prepared with self-assembly as antibody on Au NPs surface in 1.0 mmol L^{-1} $K_3Fe(CN)_6$+$K_4Fe(CN)_6$ containing 0.1 mol L^{-1} KCl.

In order to further elucidate the unidirectional covalence between AFB1 antibody and L-cysteine, the obtained sensor was used to test the same AFB1solution when only the AFB1 antibody was activated, and a smaller change in Ret was obtained compared to that of the bidirectional covalence (Fig. 3C), revealing that bidirectional covalence can enhance the amount of AFB1 antibody, which resulted the response inreasing. Meanwhile, when AFB1 antibody was directly self-assembled on the Au NPs-P-N-r-GO / GCE surface with same method as the previous reports [12, 18], the sensor presented a smaller response than that of covalence (Fig. 3D) indicating that the covalence strategy offers more advantages. For this strategy, P-N-r-GO provided large specific surface area to electrodeposit massive Au NPs. Thus, more L-cysteine could be self-assembled onto Au NPs surface, and its amino group and carboxyl group were simultaneously used to covalently combine AFB1 antibody, which enhanced the amount of AFB1 antibody, resulting the obtained sensor presented best response for AFB1 than that of others.

3.3 Optimization of experimental variables for the electrochemical immunosensor

3.3.1 Effect of Electrodeposition time of Au NPs

Electrodeposition time of Au NPs for the construction of sensor was considered in the range of 10 ~ 30 s (Fig. S3A). It was found Ret of the sensor increased with the electrodeposition time, and reached a maximum value at 20 s, followed by a gradual decrease. This non-monotonic behavior was attributable to the difference in the amount of Au NP. When the amount of Au NPs increased with electrodeposition time, their size also increased resulting in a reduced specific area, which made the amount of AFB1 antibody on the electrode surface decreased, consequently, a decreased response. Thus, 20 s was chosen as the optimal time for the electrodeposition of Au NPs for the construction of the sensor.

3.3.2 Effect of AFB1 antibody concentration

To discuss the effect of AFB1 antibody concentration on the sensor, the concentration was changed from 50 μg mL^{-1} to 160 μg mL^{-1} (Fig. S3B). The results demonstrated that the Ret increased with increasing concentration between 50 ~ 150 μg mL^{-1}. With further increase in the concentration, the Ret gradually leveled off indicating that while the antibody concentration affects the amount of AFB1 antibody on the electrode surface, it saturates after reaching a threshold as the amount of L-cysteine was fixed. 150 μg mL^{-1} antibody was chosen as the optimal concentration to construct sensor.

3.3.3 Effect of immunoreaction time for sensor

The immunoreaction time for sensor was investigated in the range of 10 ~ 60 min (Fig. S3C). The response increased with increasing time, reaching equilibrium at 50 min, revealing the completion of the immunoreaction at the sensing surface for 2.5 ng mL^{-1} AFB. To ensure the reaction proceeds successfully at lower concentrations, the immunoreaction time was increased to 70 min.

3.4 Optimal response of electrochemical immunosensor

AFB1 anti-L-cysteine-Au NPs-P-N-r-GO / GCE was used to study the response of the immunosensor at different concentrations of AFB1 under the above-mentioned optimal conditions, and the results of EIS measurements were given in Fig. 4A. The Ret increased with concentration, and exhibited a linear response in the range of 0.01 ng mL^{-1} to 10 ng mL^{-1} with Z'(Ω) = 5153 + 2527 C (ng mL^{-1}), r^2= 0.9961) (Fig. 4B). The detection limit was found to be 0.001 ng mL^{-1} (S/N= 3). This sensor exhibited a reasonable linear range and a lower detection limit for AFB1 in comparison to other electrochemical sensors [12-15, 27] and HPLC-MS methods [2, 3], which was illustrated in Table 1 in detail.

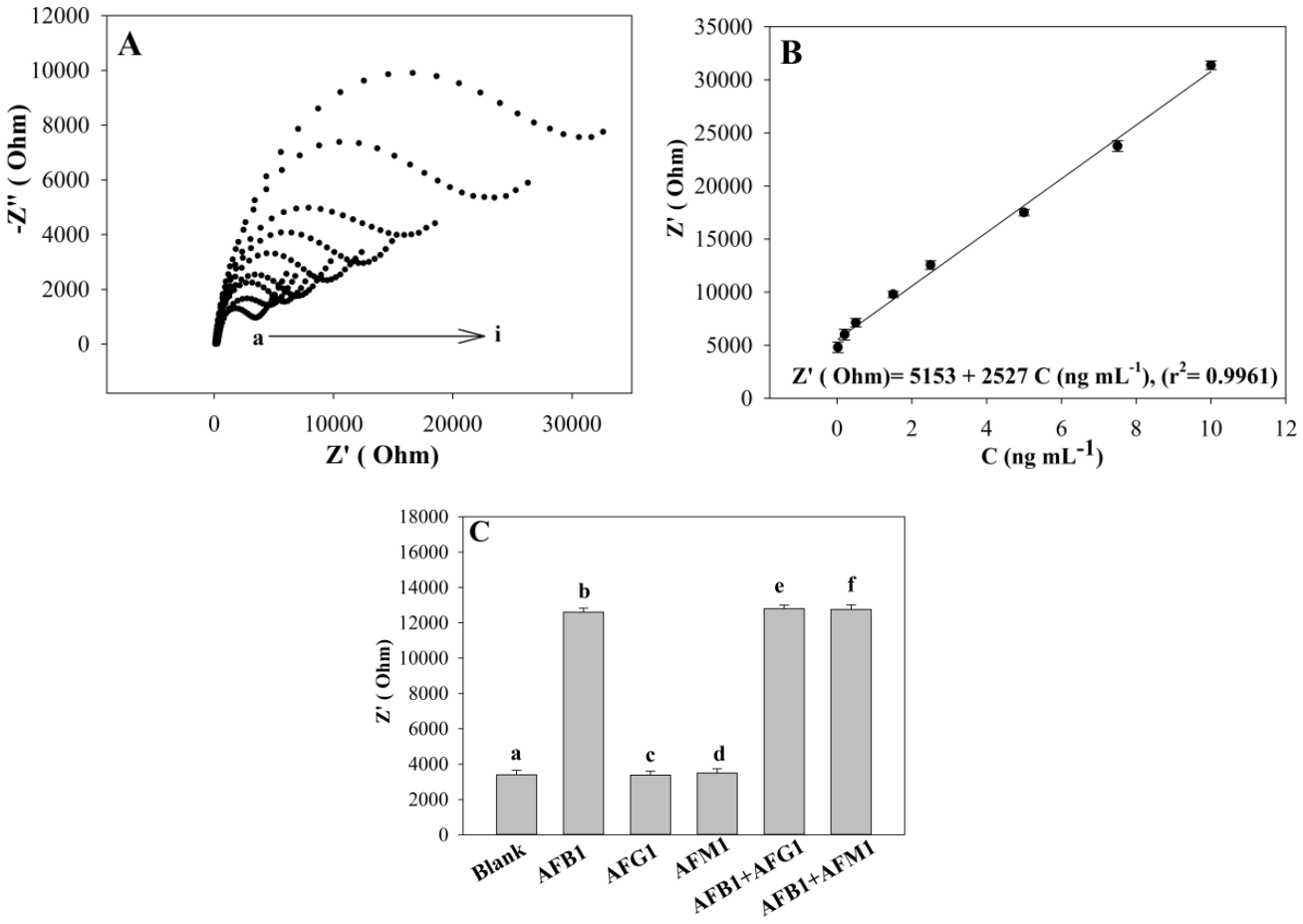

Figure 4. (A) EISs of anti-Au NPs-P-N-r-GO / GCE in 1.0 mmol L^{-1} $K_3Fe(CN)_6$+$K_4Fe(CN)_6$ containing 0.1 mol L^{-1} KCl after binding different AFB1 concentrations in the range of 0 (a) ~ 10 ng mL^{-1} (i). (B) The calibration curve anti-Au NPs-P-N-r-GO / GCE for AFB1. Error bars represented SD (n=3). (C) Effect of similar compounds on the Ret response of AFB1. Error bars represent SD (n=3). Solution composition: (a) 0 mol L^{-1} AFB1, (b) 2.5 ng mL^{-1} AFB1, (c) 25 ng mL^{-1} AFG1, (d) 25 ng mL^{-1} AFM1, (e) b + 25 ng mL^{-1} AFG1 and (f) b + 25 ng mL^{-1} AFM1.

Table 1. Comparison between the proposed immunosensor with those reported in the literatures for AFB1 detection.

Method	Linear range (ng mL^{-1})	Detection limit (ng mL^{-1})	Ref.
HPLC-MS	0.5 ~ 25	0.5	[2]
HPLC-MS	0.005 ~ 4.53	0.005	[3]
Anti-Pd-Au nanoparticles supported on functionalized PDDA-MWCNT	0.05 ~ 25	0.03	[12]
Anti-reduced graphene oxide modified electrode	0.125 ~ 1.50	0.12	[13]
Aptamer-polythiophene-3-carboxylic acid	2.5 ~ 30	1.60	[14]
Anti-mesoporous carbon (luminol-AgNPs@MC)	0.05 ~ 50	0.005	[15]
Anti-chitosan-gold NPs	0.1 ~ 30	0.06	[27]
Anti-L-cysteine-Au NPs / P-N-r-GO	0.01 ~ 10	0.001	This work

Note:
PDDA-MWCNT: Carbon nanotubes/poly(diallyldimethylammoniumchloride)
MC: Mesoporous carbon

3.5 Selectivity of electrochemical immunosensor

AFG1 and AFM1 were chosen as interferences to estimate the selectivity of the immunosensor (Fig. 4C). When it was used to detect 2.5 ng mL^{-1} AFB1, Ret of the sensor was measured to be 12205 Ω result in an obvious response. Meanwhile, when it was used to test AFG1 and AFM1, the response was only slightly different from a blank response. On the other hand, when it was used in the presence of AFB1 and 10-fold AFG or AFM1, the response was mainly caused by AFB1 indicating the selectivity of the sensor for AFB1.

3.6 Stability and repeatability

Repeatability and stability are the key factors for the immunosensor. Consequently, 2.5 ng mL^{-1} AFB1 was tested for five successive assays, and its variation coefficient was found to be 4.8%. After 10 successive assays, its Ret maintained 97.90% of its initial value. When it was not used and maintained in PBS (pH= 7.2) at 4 ℃ for 10 days, the Ret still maintained up to 96.58% (RSD= 5.6%, n= 5) of its initial value indicating the acceptable stability of the sensor. To evaluate its repeatability, five different electrodes were fabricated independently at the same conditions, and used to test 2.5 ng mL^{-1} AFB1. A root square deviation (RSD) of 5.1%, was obtained, verifying the repeatability of the fabrication procedure.

3.7 Detection of real samples

The obtained electrochemical immunosensor was employed to test AFB1 in peanuts. Firstly, the peanut sample was treated following previous work **[**28**]** with slight modifications as described in

SI. The results were shown in Table 2 which were in agreement with the ultra-HPLC-MS method [28**]** as detailed in **SI**, indicating the immunosensor could be used to test AFB1 in real samples.

Table 2. Assay results of samples using the obtained immunosensor and ultra-HPLC-MS

Samples	Immunosensor		Ultra-HPLC-MS	
	Found (ng mL^{-1})	RSD(%, n=5)	Found (ng mL^{-1})	RSD (%, n=5)
1	0.053	4.1	0.058	5.8
2	0.065	4.8	0.069	5.1
3	0.042	2.6	0.047	6.4

4. CONCLUSION

In this work, 4-aminopyrazolo[3,4-d]pyrimidine was used as a novel nitrogen source to prepare N-r-GO using the hydrothermal method, and HNO_3 was used to oxidize N-r-GO to form a porous and three-dimensional structure enhancing the specific area. Then, Au NPs were electrodeposited on P-N-r-GO to bind L-cysteine. As a result, bidirectional covalent reaction occurred between the amine and carboxyl groups of L-cysteine and AFB1 antibody, which can potentially enhance the amount of antibody compared to the unidirectional strategy. Thus, this method enhanced the sensitivity of the sensor, and provided a way to detect AFB1 in real samples.

ACKNOWLEDGEMENTS
This work was jointly supported by the National Natural Science Foundation of China (Grant No. 21665008), Yunnan Province Young Academic and Technical Leaders (2018HB005), Young Academic Reserve Program of Honghe University (Grand No. 2016HB0401) and Scientific Research Fund Project of Honghe University (XJ16B04).

CONFLICTS OF INTEREST
There are no conflicts to declare.

ELECTRONIC SUPPLEMENTARY INFORMATION

1. EXPERIMENTAL DETAILS

1.1 Chemicals

All chemicals were of analytical grade and used as received. Tetrachloroauric acid ($HAuCl_4$) (99.0%), Aflatoxin B1 (99%), Aflatoxin G1 (99%) (AFG1), Aflatoxin G1 (99%) (AFM1), mouse anti-AFB1 monoclonal antibody, bovine serum albumin (BSA), N-(3-dimethylaminopropyl)-N'-ethylcarbodiimide (EDC, 99%), N-Hydroxysulfosuccinimide sodium salt (sulfo-NHS, 99%) were purchased from Sigma-Aldrich. Purified water (18 MΩ cm^{-1}) was

used in all experiments. Unless stated otherwise, other reagents were analytical grade. The peanut samples were purchased from the local supermarket. The phosphate buffer solution (PBS, pH= 7.2) was prepared with NaH_2PO_4 and Na_2HPO_4, and its concentration was 0.1 mol L^{-1}.

Graphene oxide (GO) was prepared by a modified Hummers method [25] and characterized as in our previous report [26]. Then, HNO_3 was used to oxidize it to form the porous structure. 50 mg N-r-GO was dispersed in 100 mL of 7 mol L^{-1} HNO_3 in a round-bottom flask in oil bath at 140 °C, and mixed using a magnetic stirrer and reflux for 20 min. Then, the obtained products were collected by centrifugation and washed with H_2O, followed by freeze-drying for 24 h.

1.2 Characterization

Transmission electron microscopy (TEM) images and energy dispersive spectrum (EDS) data were obtained by using a JEOL JEM-2010 transmission electron microscope, which was operated at 200 kV after placing a drop of hydrosol on carbon coated Cu grids (200 mesh). High resolution TEM images and high-angle annular dark-field scanning transmission electron microscope-energy-dispersive-X-ray spectroscopy (HAADF-STEM-EDS) was taken by a FEI TITAN transmission electron microscope operated at 300 kV. The samples aqueous suspension of samples were dropped on carbon coated Cu grids (Ted Pella, Redding, CA) using pipettes and dried under ambient condition. X-ray photoelectron spectroscopy (XPS) measurements were carried out using a Thermo VG Scientific Sigma Probe spectrometer with Al KRX-ray (1486.6 eV) as the light source. XPS data were calibrated on the C 1s peak at 284.6 eV.

To construct a three-electrode system, we employed modified glassy carbon electrode (GCE) as a working electrode, a platinum foil as counter electrode and a saturated calomel electrode (SCE) as reference electrode. Electrochemical impedance spectra (EIS) was performed with an Autolab PGSTAT302N electrochemistry workstation (Switzerland), and the frequency range was 0.1 Hz to 100 kHz.

1.3 Sample treatment [28]

A 2.5 g sample was macerated with 10 mL of 84 % acetonitrile aqueous solution for 20 min, and then homogenized for 3 min with high speed homogenizer at 14000 rpm. After extraction, the solution was centrifuged 12000 r/min for 15 min. The supernatant was transferred into a new glass tube and dried under gentle nitrogen flow at 45°C. Finally, the residue was reconstituted with 0.5 mL of methanol:water (70:30, V/V), filtered through a 0.22 μm filter, and 10 μL was injected into the UHPLC/MS/MS.

For electrochemical immunosensor, as filtered, directly injected into 9.5 mL PBS for determination.

1.4 HPLC for AFB1 [28]

HPLC analysis was performed using a Waters Acquity Ultra Performance LC system (Waters, Milford, MA, USA). Chromatographic separation was achieved using a Waters Acquity UPLC HSS T3 column (100 mm × 2.1 mm, 1.8 μm particle size; Waters, Milford, MA, USA) with a mobile phase flow rate of 0.3 mL min^{-1}. The mobile phase consisted of (A) water containing 0.1% formic acid and (B) acetonitrile/methanol (50/50, v/v). A gradient elution program was applied as follows: 0 ~ 4.2 min linearly increased from 32% to 45% B, 4.2 ~ 5.0 min linearly increased from 45% to 100% B, 5.0 ~ 5.7 min hold on 100% B, 5.7 ~ 6.0 min linearly decreased from 100% to 32% B. A subsequent re-equilibration time (3min) should be performed before next injection, giving a total run time of 9 min. The injection volume was 10 μL. Moreover, the column and sample temperature were maintained at 40 and 20 ◦C, respectively.

MS/MS was performed on a Waters Micromass Quattro Ultima Pt tandem quadrupole mass spectrometer (Micromass, Manchester, UK). The parameters used for the mass spectrometer under the ESI^+ mode were set as follows: capillary voltage of 3.50 kV, cone voltage of 45 V, source temperature of 120 °C and desolvation temperature of 350 °C. The cone and desolvation gas flow were 50 and 570 L h^{-1}, respectively. Quantitation was performed in multiple reaction monitoring (MRM) mode.

2. SUPPLEMENTARY FIGURES.

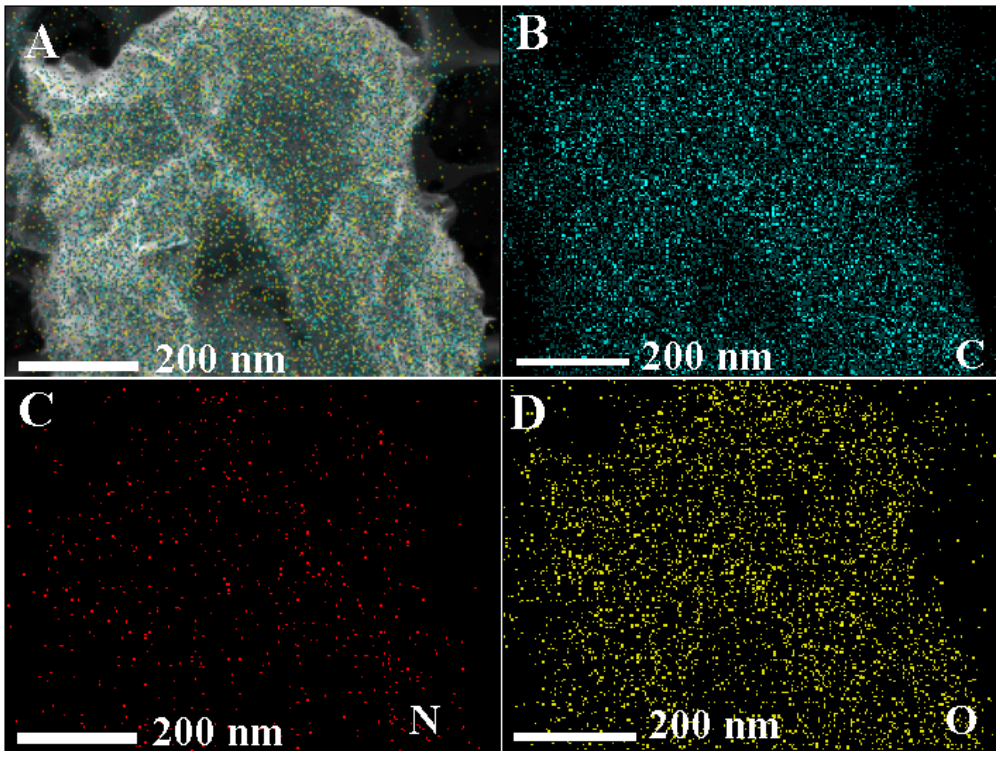

Figure S1 EDS mapping of N-r-GO

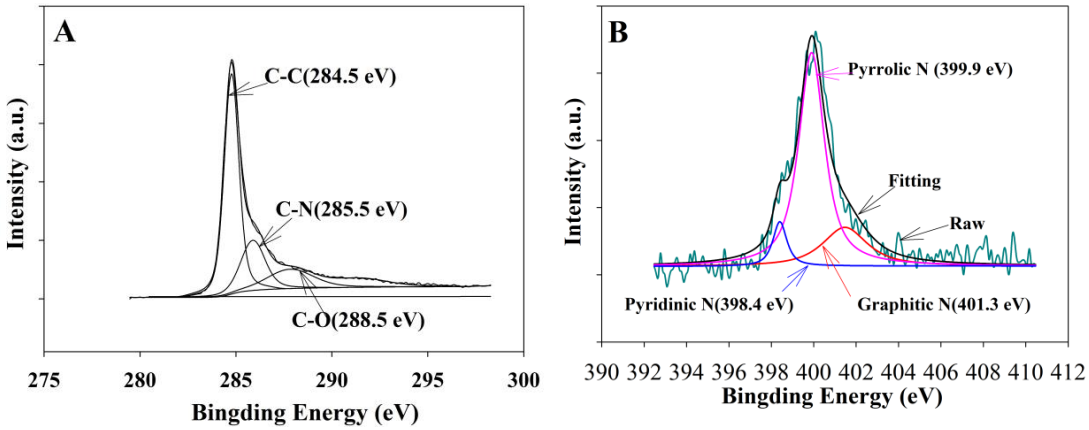

Figure S2 High resolution C1 s XPS spectra (A) and High resolution N1 s XPS spectra (B).

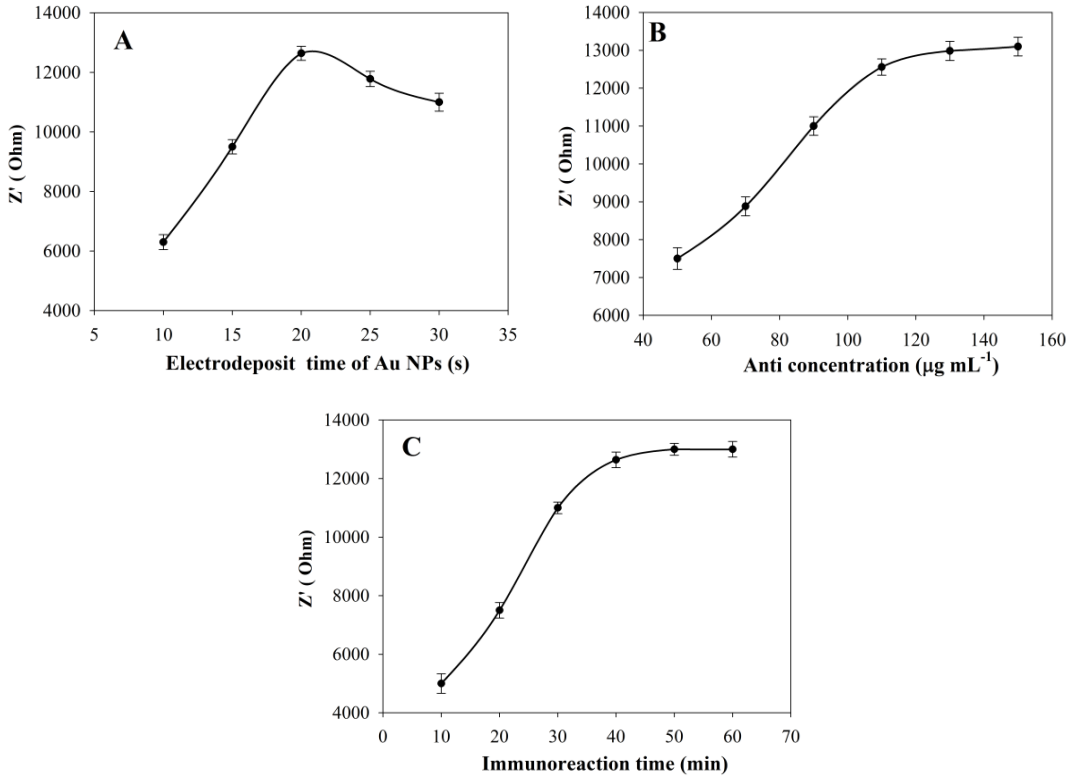

Figure S3 Effect of different factors on electrochemical immunosensor for 2.5 ng mL^{-1}. All error bars represent SD (n= 3). (A) Electrodeposite time of Au NPs; (B) Anti concentration; (C) immunoreation time.

References

1. Z. Xue, Y. Zhang, W. Yu, J. Zhang, J. Wang, F. Wan, Y. Kim, Y. Liu and X. Kou, *Anal. Chim. Acta*, 1069 (2019) 1.
2. J. L. Hidalgo-Ruiz, R. Romero-González, J. L. Martínez Vidal and A. Garrido Frenich, *Food Chem.*, 288 (2019): 22.

3. L. Izzo, Y. Rodríguez-Carrasco, J. Tolosa, G. Graziani, A. Gaspari and A. Ritieni, *J. Dairy Sci.*, 103 (2020) 1250.
4. J. Mao, N. Zheng, F. Wen, L. Guo, C. Fu, H. Ouyang, L. Zhong, J. Wang and S. Lei, *Food Control*, 84 (2018) 305.
5. B. H. Liu, Y. T. Hsu, C. C. Lu and F.Y. Yu, *Food Control*, 30 (2013) 184.
6. J. W. Liu, C. C. Lu, B. H. Liu and F. Y. Yu, *Food Control*, 59 (2016) 700.
7. Z. Linting, L. Ruiyi, L. Zaijun, X. Qianfang, F. Yinjun and L. Junkang, *Sensor Actuat. B-Chem.*, 174(2012) 359.
8. G. Evtugyn, A. Porfireva, V. Stepanova, R. Sitdikov, I. Stoikov, D. Nikolelis and T. Hianik, *Electroanalysis*, 26 (2014) 2100.
9. L. Shi, Z. Wang, G. Yang, H. Yang and F. Zhao, *Appl. Surf. Sci.*, 527 (2020) 146934.
10. D. Wang, W. Hu, Y. Xiong, Y. Xu and C. M. Li, *Biosens. Bioelectron.*, 63 (2015) 185.
11. L. Yu, Y. Zhang, C. Hu, H. Wu, Y. Yang, C. Huang and N. Jia, *Food Chem.*, 176 (2015) 22.
12. S. Zhang, Y. Shen, G. Shen, S. Wang, G. Shen and R. Yu, *Anal. Biochem.*, 494 (2016) 10.
13. S. Srivastava, V. Kumar, M. A. Ali, P. R. Solanki, A. Srivastava, G. Sumana, P. S. Saxena, A. G. Joshi and B. D. Malhotra, *Nanoscale*, 5 (2013) 3043.
14. H. Zejli, K. Y. Goud and J. L. Marty, *Sens. Bio-Sens. Res.*,25 (2019) 100290.
15. X. Lv, Y. Li, W. Cao, T. Yan, Y. Li, B. Du and Q. Wei, *Sensor Actuat. B-Chem*., 200 (2014) 53.
16. L. Chen, J. Jiang, G. Shen and R. Yu, *Anal. Methods*, 7 (2015) 2354.
17. X. Zhang, C. R. Li, W. C. Wang, J. Xue, Y. L. Huang, X. X. Yang, B. Tan, X. P. Zhou, C. Shao, S. J. Ding and J. F. Qiu, *Food Chem.*, 192 (2016) 197.
18. A. Sharma, A. Kumar and R. Khan, *Mat. Sci. Eng. C-Mater.*, 76 (2017) 802.
19. M. Kaur, M. Kaur and V. K. Sharma, *Adv. Colloid Interface Sci.*, 259 (2018)44.
20. T. Granzier-Nakajima, K. Fujisawa, V. Anil, M. Terrones and Y. T. Yeh, *J. Nanomater.*, 9 (2019) 425.
21. Z. Xing, Z. Ju, Y. Zhao, J. Wan, Y. Zhu, Y. Qiang and Y. Qian, *Sci. Rep.*, 6 (2016) 26146.
22. J. W. Lee, J. M. Ko and J. D. Kim, *Electrochim. Acta*, 85 (2012) 459.
23. H. Xu, L. Ma and Z. Jin, *J. Energy Chem.*, 27 (2018) 146.
24. P. Chen, J. J. Yang, S. S. Li, Z. Wang, T. Y. Xiao, Y. H. Qian and S. H. Yu, *Nano Energy*, 2 (2013) 249.
25. Y. Liang, D. Wu, X. Feng and K. Müllen, *Adv. Mater.*,21 (2009) 1679.
26. G. Yang and F. Zhao, *J. Mater. Chem. C*, 2 (2014) 10201.
27. L. Chen, J. Jiang, G. Shen and R. Yu, *Anal. Methods*, 7 (2015) 2354.
28. B. Huang, Z. Han, Z. Cai, Y. Wu and Y. Ren, *Anal. Chim. Acta*, 662 (2010) 62.